Electronic structures and superconductivity of endohedrally doped C_{28} solids from first principles

Nichols A. Romero,[1,*] Jeongnim Kim,[2] and Richard M. Martin[1]
[1]*Department of Physics, Materials Research Laboratory, and Materials Computation Center, University of Illinois, Urbana, Illinois 61801, USA*
[2]*NCSA, Materials Research Laboratory, and Materials Computation Center, University of Illinois, Urbana, Illinois 61801, USA*
(Received 17 April 2007; revised manuscript received 19 September 2007; published 6 November 2007)

We present *ab initio* calculations of the crystalline phases of C_{28}: hyperdiamond and hyperlonsdaleite, in their pristine and endohedrally doped forms. These are hard materials with strong covalent bonds between the C_{28} molecules, and yet their electronic properties have remarkable similarities to the weakly bonded $C_{28}H_4$ molecular solids previously investigated [Phys. Rev. B **70**, 140504(R) (2004)]. Our calculations show that they exhibit very narrow bands near the Fermi energy with an electron-phonon coupling that is well described by a molecular model and is larger than in C_{60}. Our study focuses on C_{28} solids endohedrally doped with Zr, a group-IVB tetravalent atom. Solid $Zr@C_{28}$ is a small-gap insulator with Jahn-Teller distortions. Since the two structures considered are degenerate in energy, the actual material is expected to have disorder affecting the states at the Fermi energy and leading to a nonvanishing density of states. We conclude that the small density of states at the Fermi energy for $Zr@C_{28}$ will lead to a superconducting transition temperature T_c lower than that found in K_3C_{60}; however, our results suggest that a higher T_c may be obtained using group-IIIB trivalent atoms.

DOI: 10.1103/PhysRevB.76.205405 PACS number(s): 71.20.Tx, 74.70.Wz, 74.10.+v

I. INTRODUCTION

There has been much interest in solids based on small fullerenes because of their potential for exhibiting superconducting transition temperatures T_c exceeding those found in alkali-doped C_{60}.[1] This expectation is based on arguments that the electron-phonon coupling increases with the curvature of the fullerene.[2–4] However, solids formed from the small fullerenes are difficult to synthesize because of their reactive nature. The case of C_{36} and C_{20} exemplifies the difficulties encountered in synthesizing small fullerenes. Although C_{36} has been produced under specific experimental conditions by the electric arc-discharge method,[5] its purified form spontaneously oligomerizes in the solid state.[6] Comparably difficult to synthesize is C_{20}, the smallest known fullerene. Its synthesis necessitating the use of the precursor molecule dodecahadrane $C_{20}H_{20}$, followed by chemical substitution of the hydrogen atoms with bromine atoms, and finally gas-phase debromination.[7]

In this work, we present calculations of solids based on C_{28}, the smallest fullerene to be produced in abundance in the laser vaporization of graphite,[8] a method commonly used in the production of single-wall carbon nanotubes (SWCNTs). Experiments have shown that it can be stabilized and its production enhanced by group-IVB tetravalent atoms in a manner analogous to metal catalysts enhancing the production of SWCNTs.[8] This fullerene encapsulates a single tetravalent atom (M) in its carbon cage, forming an endohedral complex $M@C_{28}$ (M=Zr, Ti, Hf, and U). The relative absence of empty C_{28} molecules suggests that this fullerene nucleates around these metallic atoms. Theoretical calculations have shown the C_{28} molecule to posses robust bonding flexibility. It is capable of forming endohedral complexes $M@C_{28}$ with tetravalent atoms, exohedral complexes $C_{28}A_4$ with univalent atoms (A), and even simultaneous bonding inside and outside the fullerene cage $M@C_{28}A_4$.[9–12] The C_{28} molecule also displays a number of hidden valencies with hydrogen: $C_{28}H_{10}$, $C_{28}H_{16}$, $C_{28}H_{22}$, and $C_{28}H_{28}$, which are as stable as $C_{28}H_4$.[13] Furthermore, it is capable of forming a number of ordered and disordered solids with similar cohesive energies.[14–18]

In our previous work,[19] we investigated several C_{28}-derived closed-shell molecules ($C_{24}B_4$, $C_{24}N_4$, and $C_{28}H_4$) as the building block for molecular solids exhibiting many of the salient features of solid C_{60}. The lowest energy $C_{24}N_4$ solid was determined to exhibit covalent bonding, while the $C_{24}B_4$ molecules were shown to be unstable in the solid. In contrast, $C_{28}H_4$ formed a *weakly interacting* molecular solid similar to C_{60}. The alkali doping of solid $C_{28}H_4$ manifested a complex behavior which does not occur in the alkali-doped C_{60} materials. This included hybridization of dopant states near the Fermi level and Jahn-Teller distortions, which lead to insulating behavior. Of the three alkali-doping scenarios considered, only the endohedral doping of $C_{28}H_4$ exhibited the nearly ideal rigid-band donor behavior that occurs in the superconducting C_{60} fullerides. The superconducting transition temperature of the solid $Na@C_{28}H_4$ was predicted to be 58 K, higher than that found in any other C_{60} fulleride to date.

Although there have been studies on isolated metallofullerenes,[9–12] we present an *ab initio* calculation of solids based on the experimentally synthesizable $M@C_{28}$ molecule. While Guo *et al.*[8] found $Hf@C_{28}$ and $U@C_{28}$ to be the most abundant endohedral complexes, we chose to study $Zr@C_{28}$ as our prototypical metallofullerene due to its simpler electronic configuration and its comparative abundance with respect to $Ti@C_{28}$ in these experiments. It is expected that solids based on other synthesizable $M@C_{28}$ molecules should behave similarly. Results on the structural and electronic properties of $Zr@C_{28}$ in the hyperdiamond and hyper-

 ©2007 The American Physical Society

TABLE I. Reference configuration and cutoff radii (r_c^ℓ) of the pseudopotentials employed in this calculation. The Zr pseudopotential was generated in the +2 ionic configuration to allow the inclusion of the 4*s* and 4*p* semicore states. Scalar-relativistic corrections were used for zirconium. The cutoff radii for Zr are taken from Giannozzi as provided in Ref. 27. Radii are reported in Bohr units.

Element	Reference configuration	r_c^s	r_c^p	r_c^d	r_c^f
C	$2s^2 2p^2 3d^0 4f^0$	1.25	1.25	1.25	1.25
Zr	$4s^2 4p^6 4d^2 5f^0$	1.35	1.43	1.55	1.65

lonsdaleite phases are presented. These are strongly bonded solids which have been shown to be stable in the pure undoped form in previous work.[14–18] The phases are determined to be isoenergetic and share many common features with the previously studied C_{28}-derived solids. We conclude with an assessment of superconductivity in these endohedrally doped materials.

II. METHODOLOGY

Our calculations are performed within the local density approximation[20] (LDA) to Kohn-Sham density-functional theory[21] as implemented in the SIESTA code.[22,23] The LDA uses the Perdew-Zunger[24] parametrization of the Ceperley-Alder[25] exchange-correlation energy for the homogeneous electron gas. The core electrons were replaced with norm-conserving pseudopotential generated using the Troullier-Martins scheme.[26] The reference configuration and cutoff radii used for the carbon (C) and zirconium (Zr) pseudopotentials are listed in Table I. In order to maximize transferability within the Troullier-Martins scheme, the Zr pseudopotential was generated using +2 ionic configuration in order to allow the inclusion of the 4*s* and 4*p* semicore states.

The single-particle Kohn-Sham eigenstates were expanded in a basis of strictly localized numerical atomic orbitals. The basis functions were obtained by finding the eigenfunctions of the isolated atoms in a soft-confining potential.[28] A double-ζ plus polarization basis set was used for the valence states of all the atoms, while a double-ζ basis set was used for the 4*s* and 4*p* semicore states of zirconium.[29] The parameters which define the range and shape of the basis functions for C and Zr were obtained by variational optimization in C_{60} and hcp Zr, respectively, according to the method described in Ref. 28.

An equivalent plane-wave cutoff of 200 Ry was used to represent the charge density on the real-space grid. The Brillouin zone was sampled using $2\times2\times2$ and $2\times2\times1$ Monkhorst-Pack[30] (MP) grids for hyperdiamond and hyperlonsdaleite, respectively, since the latter unit cell is twice in length along the *c*-axis direction. When the zone sampling was increased to shifted MP grids of $4\times4\times4$ and $4\times4\times2$ for the hyperdiamond and hyperlonsdaleite structures, respectively, the differences in the total energies were less than 5 meV/atom in both the pristine and Zr-doped cases.

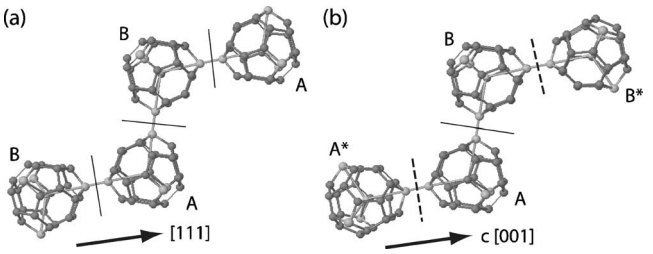

FIG. 1. $Zr@C_{28}$ molecules in the apex-bonded (a) hyperdiamond and (b) hyperlonsdaleite structures along the [111] and *c*-axis [001] directions, respectively. The apex and dopant atoms are shown in a lighter shading. The planes of inversion and reflection about the bond center are depicted by solid and dotted lines, respectively. Hence, molecule pairs AB and A^*B^* are each inversions, while AA^* and BB^* are each reflections.

III. STRUCTURE OF THE SOLID

We consider two possible structures where there are strong covalent bonds between the apex atoms of neighboring molecules. In addition to the apex-bonded hyperdiamond structure considered in our previous work,[19] the apex-bonded hyperlonsdaleite phase of Seifert *et al.*[31] is also investigated. Hyperdiamond and hyperlonsdaleite are essentially cubic and hexagonal diamond, respectively, with a molecule of compatible symmetry for a basis. These are fourfold coordinated crystal structures with first-nearest neighbors that are identical except for the relative orientation of the constituent molecules. Figure 1 depicts the different orientations along the [111] direction in hyperdiamond and its equivalent direction along the *c* axis [001] in hyperlonsdaleite. The unit cells are characterized by two (AB) and four (ABB^*A^*) molecules for hyperdiamond and hyperlonsdaleite, respectively. In the hyperdiamond structure, all four nearest neighbors (B) are an inversion of the original molecule (A) about the bond center, while in the hyperlonsdaleite structure the nearest neighbor *parallel* to the *c* axis (A^* or B^*) is a reflection, with the other three neighbors being inversions as in hyperdiamond.[32] The total energies of apex-bonded hyperdiamond and hyperlonsdaleite are expected to be similar from a simple tight-binding picture since the first-nearest neighbors are identical, except for relative orientations, and contributions from second and higher nearest neighbors would be negligible. This is quite different from the case of carbon diamond and lonsdaleite, where the length scale between first- and second-nearest neighbors are of the same order, resulting in distinct electronic and physical properties for the two phases.

For both the hyperdiamond and hyperlonsdaleite structures, the $Zr@C_{28}$ molecules are able to bond in either the apex-bonded or face-bonded configuration as described in Ref. 19. Unlike the case of the $C_{28}H_4$ where the apex-bonded hyperdiamond was not possible due to the steric hindrance of the hydrogen atoms, both structures are feasible with C_{28} and $Zr@C_{28}$. The face-bonded structures are a family of weakly interacting molecular solids, while the apex-bonded structures are strongly bonded *covalent* solids. The apex-bonded structures are much lower in energy than their face-bonded counterparts. In the case of hyperdiamond C_{28}, the apex-

TABLE II. Properties of C_{28} and $Zr@C_{28}$ in the hyperdiamond (dia) and hyperlonsdaleite (lons) structures. Binding energies and lattice constants are in eV/molecule and Å units, respectively. The reference binding energies for the solids are obtained from spin-polarized calculations on the isolated constituent molecule.

	Binding energy		a		c/a
Molecule	dia	lons	dia	lons	lons
C_{28}	6.2	6.1	15.80	11.18	1.64
$Zr@C_{28}$	1.7	1.6	16.05	11.31	1.65

bonded structure was at least 11 eV/molecule lower in energy than the face-bonded version.

Because the face-bonded structures are much higher in energy, we focus our study on apex-bonded hyperdiamond and hyperlonsdaleite. By using SIESTA, these structures in their pristine and endohedrally doped forms were relaxed until the forces on the atoms did not exceed 0.04 eV/Å and the stress on the unit cell was within 0.2 GPa of zero pressure. For the endohedrally doped solids which exhibited very small gaps, an electronic temperature $T_{el}=5.44$ meV (0.2 mhartree) was used. Smaller values of T_{el} did not alter our minimum energy structures within the aforementioned tolerances.

Our calculations determined that the hyperdiamond and hyperlonsdaleite structures are degenerate to within a few meV/atom, which exceeded the degree to which the total energy is converged. The binding energies for these structures are reported in Table II. This result is not surprising given that the first-nearest neighbors in hyperdiamond and hyperlonsdaleite structures are identical except for their orientation. Even though the second-nearest neighbors are distinct, these interactions would not effect the total energy given the negligible overlap due to the large distances involved. Since bonding in these two structures is expected to be very similar and calculations show that they are degenerate, one would expect the presence of orientational disorder analogous to that found in the C_{60} solids.[33] This disorder will have ramifications for estimates of T_c, which are discussed later in Sec. V.

The equilibrium lattice parameters for C_{28} and $Zr@C_{28}$ are given in Table II. The lattice parameters of C_{28} in the hyperdiamond and hyperlonsdaleite structures are in good agreement with those obtained by Seifert *et al.* using their density-functional-based tight-binding method.[15,16] There is a small expansion of the lattice in both the hyperdiamond and hyperlonsdaleite structures upon endohedral doping with zirconium. The smaller binding energies for the $Zr@C_{28}$ solids reflect the weaker bonding as a result of the internally passivated dangling bonds.

IV. ELECTRONIC PROPERTIES OF THE SOLID

A. Solid C_{28} and $C_{28}H_4$

Kaxiras *et al.*[17] showed that the highest occupied molecular orbital (HOMO) and lowest unoccupied molecular orbital (LUMO) of C_{28}, which are dangling bond states, are formed from combinations of the atomic orbitals centered on the apex atoms. They argued that the C_{28} HOMO (LUMO) end up far below (above) the Fermi level upon formation of the hyperdiamond solid. The states which end up far below the Fermi level form the strong covalent bonds between the apex atoms of C_{28} in the solid. Although there are no covalent bonds present in solid $C_{28}H_4$, hydrogen passivation of the dangling bonds leads to a similar effect. It then follows that the valence (conduction) band of solid C_{28} are formed from states which are similar to the HOMO (LUMO) of $C_{28}H_4$, and not C_{28}; these are π states localized on the four hexagons.

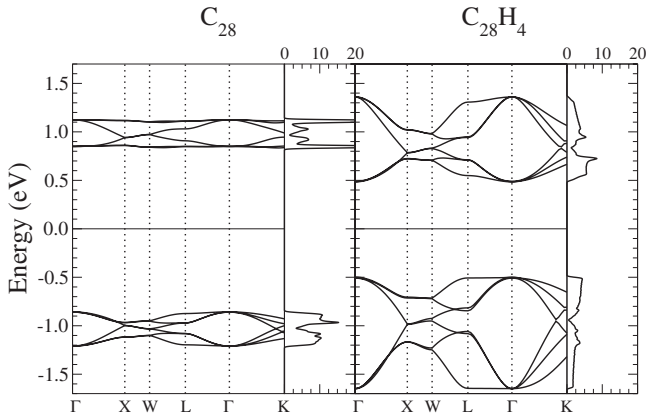

FIG. 2. Band structure and DOS (states/eV/spin/molecule) of apex-bonded C_{28} and face-bonded $C_{28}H_4$ hyperdiamond. There are two molecules per unit cell. The thin solid line at zero is the Fermi level. The band structure and DOS for face-bonded $C_{28}H_4$ are taken from Ref. 19.

Figure 2 provides convincing evidence supporting this notion. This figure compares the band structure and density of states (DOS) between apex-bonded C_{28} and face-bonded $C_{28}H_4$ in the hyperdiamond structure. The DOS for C_{28} was generated by Gaussian smearing with $\sigma=10$ meV and a $12\times12\times12$ MP grid using the converged self-consistent charge density obtained with a $2\times2\times2$ MP grid. The similarity between their band structures is particularly pronounced in the valence band of these two materials along the high symmetry lines in the Brillouin zone (BZ). Hence, one concludes that in solid C_{28} and $C_{28}H_4$, the bands near ε_F are formed out of the same π states localized on the hexagons of the constituent molecule, with differences in the band structure arising from different bonding configurations, apex bonded for C_{28} and face bonded for $C_{28}H_4$. The hydrogen passivation of C_{28} eliminates the dangling bond states, localized on the apex atoms, near the Fermi level in the same manner as the formation of the covalent bonds in the case of solid C_{28}. The bands are broader in the face-bonded $C_{28}H_4$ compared to the apex-bonded C_{28} due to the proximity of the hexagons in the former, which leads to a greater overlap of the π states. In summary, the bands near the Fermi level of solid C_{28} and solid $C_{28}H_4$ are *both* formed from the HOMO and LUMO of $C_{28}H_4$. We will return to this important point in Sec. V when we proceed to calculate T_c in the $Zr@C_{28}$ solids.

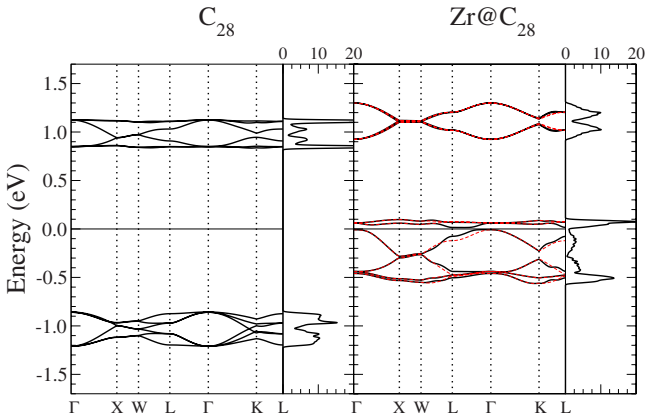

FIG. 3. (Color online) Band structure and DOS (states/eV/spin/molecule) of apex-bonded hyperdiamond: C_{28} and $Zr@C_{28}$. There are two molecules per unit cell. The thin solid line at zero is the Fermi level. The dashed red lines in the band structure plot are the same set of bands plotted along the distorted ⟨111⟩ direction, which has been mapped unto the same L point in this figure for simplicity. The additional symmetry line K-L is plotted.

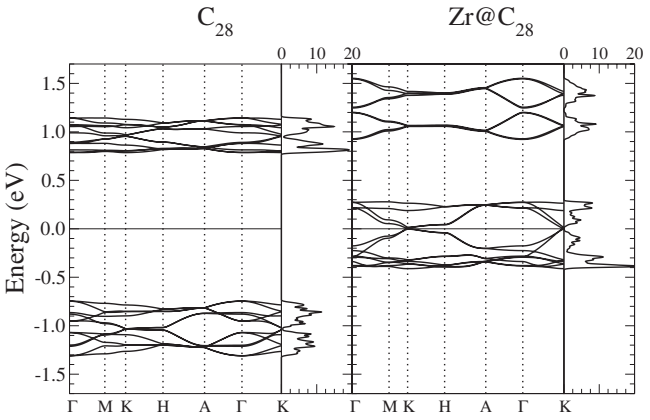

FIG. 4. Band structure and DOS (states/eV/spin/molecule) of apex-bonded hyperlonsdaleite: C_{28} and $Zr@C_{28}$. There are four molecules per unit cell. The thin solid line at zero is the Fermi level.

B. Hyperdiamond: C_{28} and $Zr@C_{28}$

Undoped C_{28} hyperdiamond is found to be an insulator with a 1.70 eV direct gap at Γ.[34] In comparison, the $Zr@C_{28}$ hyperdiamond is also insulating, but exhibiting a much smaller indirect gap of approximately 14 meV.[35] Figure 3 shows that although the conduction band of $Zr@C_{28}$ hyperdiamond retains many of the symmetries from its pristine counterpart, there are clearly others which have been lost. The most prominent of which is that the topmost set of bands are no longer degenerate at Γ. In our calculation, a very small (0.01 Å) elongation of the $Zr@C_{28}$ molecule along one of the ⟨111⟩ directions is found. It is believed that the presence of very flat bands at the top and bottom of the C_{28} conduction band leads to a Jahn-Teller distortion that results in the loss of degeneracy at Γ.

While the undoped solid has two sharp peaks in the DOS near the top and bottom of the conduction band, the Zr-doped solid features a somewhat broader DOS along with an increase in the conduction band width from 0.27 to 0.52 eV (including the topmost bands which split off) as measured at Γ. The DOS shows that upon endohedral doping, the Fermi energy falls on the edge of a narrow DOS peak. This small value for $N(0)$ observed in Fig. 3 (and also later in Fig. 4) is a consequence of the finite values for the MP grid and σ; denser MP grids with smaller smearing temperatures would give $N(0)=0$. We note that disorder in real samples of solid $Zr@C_{28}$ would result in a nonzero value of $N(0)$.

The distortion of the $Zr@C_{28}$ molecule, which leads to the formation of a small gap in the band structure of the solid, alludes to a further similarity with the alkali-doped cases of solid $C_{28}H_4$. In our previous work,[19] we found that an isolated charged $C_{28}H_4$ molecule exhibited a Jahn-Teller distortion, leading to the splitting of the threefold degenerate LUMO and creating a 0.2 eV gap. Upon formation of the alkali-doped solid, we found that $Na_2C_{28}H_4$ and $Na@C_{28}H_4$ were the extreme cases of the competition between energy gained from band broadening and that gained from a Jahn-Teller distortion of the molecule, respectively. In the $Na_2C_{28}H_4$, the Jahn-Teller distortion of the constitutive molecule lowered the energy more, and so the doped solid exhibited an insulating behavior. In contrast, the band broadening in $Na@C_{28}H_4$ lowered the energy more, and so the doped solid was metallic.

In order to elucidate the nature of these Jahn-Teller distortions in the $Zr@C_{28}$ solids, we performed calculations on the isolated $Zr@C_{28}H_4$ molecule. As argued in Sec. IV A, it is $Zr@C_{28}H_4$ and *not* $Zr@C_{28}$ that possesses the corresponding electronic structure found in these covalently bonded solids. We find that the isolated $Zr@C_{28}H_4$ molecule exhibits a 0.44 eV gap and a more pronounced Jahn-Teller distortion (0.10 Å) of its T_d symmetry than that found in $C_{28}H_4^{-1}$ (0.01 Å). In addition to the $T_d \rightarrow D_{2d}$ distortion of the molecule which was reported in our earlier work,[19] we also identify a distortion of the hexagons from $C_{6d} \rightarrow C_{2h}$. Both of these Jahn-Teller distortions are present in the isolated $Zr@C_{28}H_4$ and $C_{28}H_4^{-1}$ molecules. However, neither of these Jahn-Teller distortions are observed in the $Zr@C_{28}$ hyperdiamond, except for the previously mentioned elongation along one of the ⟨111⟩ directions.

C. Hyperlonsdaleite: C_{28} and $Zr@C_{28}$

Figure 4 compares the band structure and DOS between pristine and Zr-doped C_{28} hyperlonsdaleite.[36] The bands appear very different from those of the hyperdiamond structure (Fig. 3) since hyperlonsdaleite is hexagonal and has twice as many molecules in its unit cell. Nevertheless, one can see that the nature of the states are essentially the same by comparing properties that depend on the crystal symmetry. For instance, the DOS exhibits double peaks near the edges of the valence and conduction bands. Undoped C_{28} hyperlonsdaleite is insulating with a 1.53 eV direct gap at Γ, which is close to that found in the hyperdiamond structure.[37] The width of the conduction band as measured at the Γ point increases from 0.36 to 0.66 eV upon doping, which is comparable to the enhancement found in the hyperdiamond case

(from 0.27 to 0.52 eV). As stated in Sec. III, this is not unexpected given the similarity in structure and bonding.

Similar to $Zr@C_{28}$ hyperdiamond, the hyperlonsdaleite structure is an insulator with a small direct gap of 6 meV at K. We also find a distortion of the T_d symmetry of each molecule; this time an elongation of 0.06 Å along the c axis, which is a direction equivalent to $\langle 111 \rangle$ in the hyperdiamond structure. Interestingly, the Jahn-Teller distortion $C_{6d} \rightarrow C_{2h}$ of the hexagon faces on the $Zr@C_{28}$ molecule is present in the hyperlonsdaleite structure although it was not observed in the case of hyperdiamond. This is observed only on three of the four hexagons of each $Zr@C_{28}$ and *not* on the hexagon which face the c axis. In summary, we find a number of parallels between the electronic structure of hyperdiamond and hyperlonsdaleite in both their pristine and endohedrally doped forms. These include the structure of the DOS near the Fermi energy, insulating behavior in their pristine form, and Jahn-Teller distortions leading to small-gap (nearly semimetallic) behavior in the endohedrally doped form.

V. VIABLE METALLIC BEHAVIOR AND SUPERCONDUCTIVITY

Because the C_{28} solids considered here are covalent and not weakly interacting molecular solids like C_{60} and $C_{28}H_4$, the dimensionless electron-phonon coupling λ is most accurately determined by integrating the electronic and phononic states over the BZ, instead of the molecular like approximation which is typically used for fullerene-based solids.[3,19,38,39] However, Spagnolatti *et al.*[40] demonstrated that the molecular approximation overestimated λ by only about 10% for the covalently bonded C_{20} solid. Hence, similar errors can be expected in a molecular like approximation to λ for these C_{28} solids, which is sufficient for an estimate of T_c.

As discussed in Sec. IV A, the similarity between the band structure of apex-bonded C_{28} and face-bonded $C_{28}H_4$ hyperdiamond led to the conclusion that the bands near the Fermi level are formed from the molecular states of $C_{28}H_4$. Hence, $V_{ep}=\lambda/N(0)$ for doped C_{28} and $C_{28}H_4$ should be nearly equal in value. The other critical quantity determining λ is the density of states at the Fermi energy $N(0)$. Our calculations determined that it is essentially zero for the hyperdiamond and hyperlonsdaleite structures. This was due to the presence of very flat bands which led to Jahn-Teller distortions, creating small gaps in the band structures of the solids. Orientational disorder in the actual samples of the material can be expected to close the small band gap and lead to a nonvanishing DOS, as argued to occur in C_{60} solids.[1,41]

However, it is preferable to avoid these Jahn-Teller distortions by controlled doping of the C_{28} material. The presence of flat bands at the bottom and top of the conduction band would lead to essentially the same behavior for electron doping with a $1e$, $2e$, $4e$ (e.g., Zr), or even $5e$ atom. Doping levels larger than $2e$ but less than $4e$ per C_{28} are less likely to exhibit this behavior and result in a larger $N(0)$. These doping levels may be achieved by stoichiometric mixtures of $M@C_{28}$ with distinct endohedral atoms of different valences. Another simple scenario would be to endohedrally dope with a trivalent group-IIIB atom. The $Sc@C_{28}$ molecule has a favorable binding energy at the Hartree-Fock level of theory,[11] and experiments[42] on Y/Sc/graphite soot suggest that the formation of these metallofullerene should be possible.

VI. CONCLUSIONS

We have presented density-functional calculations on endohedrally doped C_{28} solids. Crystal structures based on $Zr@C_{28}$ are of particular interest since the molecule has been experimentally observed.[8] The most stable forms found in our work are apex-bonded hyperdiamond and hyperlonsdaleite, which have different orientations of the C_{28} molecules; since the total energies are essentially degenerate in both their pristine and there endohedrally doped forms, this suggests that disorder may persist at low temperatures in these materials, as it does in the C_{60} solids.[1,33,41]

Although these C_{28}-based solids are covalently bonded, they still share striking similarities with the weakly interacting $C_{28}H_4$ solids we previously studied.[19] For example, in the alkali-doping scenarios considered for solid $C_{28}H_4$, the competition between energy gained by a Jahn-Teller distortion of the molecule and that from band broadening lead to insulating ($Na_2C_{28}H_4$) vs metallic ($Na@C_{28}H_4$) behavior. Although the relevant constitutive molecule ($Zr@C_{28}H_4$) exhibits a pronounced Jahn-Teller distortion, none of the $Zr@C_{28}$ solids investigated here exhibited the full Jahn-Teller distortions found in the molecule. We believe that the strong covalent bonding present in these solids make them more resilient against Jahn-Teller distortion than the weakly interacting counterparts based on $C_{28}H_4$.

The resemblance between the band structure of apex-bonded C_{28} and face-bonded $C_{28}H_4$ hyperdiamond led us to conclude that electronic states near the Fermi surface are derived from the same LUMO and HOMO states of $C_{28}H_4$. We argue that V_{ep} for these two different classes of materials should be quantitatively similar. Because solids based on $Zr@C_{28}$ were determined to be small-gap insulators, we considered different doping levels that could lead to metallic behavior with larger values of $N(0)$. The presence of very flat degenerate bands in the conduction band of apex-bonded C_{28} hyperdiamond suggested that other doping levels would also lead to an insulating behavior or a small DOS with a low T_c. The most likely candidates for metallic behavior and superconductivity with higher T_c are formed from $M@C_{28}$, where M is a trivalent atom that donates $3e$ per molecule to the C_{28} solid.

ACKNOWLEDGMENTS

We are indebted to J. Junquera for providing us the computational means to optimize our basis set according to the method described in Ref. 28. This work was supported by National Science Foundation Grant No. DMR-0325939 and by the U.S. Department of Energy under Contract No. DEFG02-91ER45439. This work utilized the NCSA IBM pSeries 690 and the San Diego Supercomputing Center IBM Datastar.

*Present address: U.S. Army Research Laboratory, Aberdeen Proving Ground, MD 21005-5066.
[1] O. Gunnarsson, Rev. Mod. Phys. **69**, 575 (1997).
[2] V. H. Crespi, Phys. Rev. B **60**, 100 (1999).
[3] M. Schluter, M. Lannoo, M. Needels, G. A. Baraff, and D. Tománek, Phys. Rev. Lett. **68**, 526 (1992).
[4] J. L. Martins, Europhys. News **23**, 32 (1992).
[5] C. Piskoti, J. Yarger, and A. Zettl, Nature (London) **393**, 771 (1998).
[6] A. Koshio, M. Inakuma, T. Sugai, and H. Shinoahara, J. Am. Chem. Soc. **122**, 398 (2000).
[7] H. Prinzbach, A. Weiler, P. Landenberger, F. Wahl, J. Wörth, L. T. Scott, M. Gelmont, D. Olevano, and B. v. Issendorff, Nature (London) **407**, 60 (2000).
[8] T. Guo, M. D. Diener, Y. Chai, M. J. Alford, R. E. Haufler, S. M. McClure, T. Ohno, J. H. Weaver, G. E. Scuseria, and R. E. Smalley, Science **257**, 1661 (1992).
[9] M. R. Pederson and N. Laouini, Phys. Rev. B **48**, 2733 (1993).
[10] Y. N. Makurin, A. A. Sofronov, A. I. Gusev, and A. L. Ivanovsky, Chem. Phys. **270**, 293 (2001).
[11] T. Guo, R. E. Smalley, and G. E. Scuseria, J. Chem. Phys. **99**, 352 (1993).
[12] K. Jackson, E. Kaxiras, and M. R. Pederson, Phys. Rev. B **48**, 17556 (1993).
[13] C. Milani, C. Giambelli, H. E. Roman, F. Alasia, G. Benedek, R. A. Broglia, S. Sanguinetti, and K. Yabana, Chem. Phys. Lett. **258**, 554 (1996).
[14] J. Kim, G. Galli, J. W. Wilkins, and A. Canning, J. Chem. Phys. **108**, 2631 (1998).
[15] D. Porezag, T. Frauenheim, T. Köhler, G. Seifert, and R. Kaschner, Phys. Rev. B **51**, 12947 (1995).
[16] G. Seifert, D. Porezag, and T. Frauenheim, Int. J. Quantum Chem. **58**, 185 (1996).
[17] E. Kaxiras, L. M. Zeger, A. Antonelli, and Y. M. Juan, Phys. Rev. B **49**, 8446 (1994).
[18] D. M. Bylander and L. Kleinman, Phys. Rev. B **47**, 10967 (1993).
[19] N. A. Romero, J. Kim, and R. M. Martin, Phys. Rev. B **70**, 140504(R) (2004).
[20] W. Kohn and L. J. Sham, Phys. Rev. **140**, A1133 (1965).
[21] P. Hohenberg and W. Kohn, Phys. Rev. **136**, B864 (1964).
[22] P. Ordejón, E. Artacho, and J. M. Soler, Phys. Rev. B **53**, R10441 (1996).
[23] J. M. Soler, E. Artacho, J. D. Gale, A. García, J. Junquera, P. Ordejón, and D. Sánchez-Portal, J. Phys.: Condens. Matter **14**, 2745 (2002).
[24] J. P. Perdew and A. Zunger, Phys. Rev. B **23**, 5048 (1981).
[25] D. M. Ceperley and B. J. Alder, Phys. Rev. Lett. **45**, 566 (1981).
[26] N. Troullier and J. L. Martins, Phys. Rev. B **43**, 1993 (1991).
[27] J.-P. Crocombette and D. Ghaleb, J. Nucl. Mater. **257**, 282 (1998).
[28] J. Junquera, O. Paz, D. Sánchez-Portal, and E. Artacho, Phys. Rev. B **64**, 235111 (2001).
[29] The basis set parameters can be downloaded from the SIESTA online database.
[30] H. J. Monkhorst and J. D. Pack, Phys. Rev. B **13**, 5188 (1976).
[31] G. Seifert, A. N. Enyashin, and T. Heine, Phys. Rev. B **72**, 012102 (2005).
[32] An inversion is defined to be a transformation taking $(x,y,z) \rightarrow (-x,-y,-z)$, while a reflection is only a transformation of one of the three coordinates, e.g., $(x,y,z) \rightarrow (x,y,-z)$.
[33] J. P. Lu, X. P. Li, and R. M. Martin, Phys. Rev. Lett. **68**, 1551 (1992).
[34] In our calculation, the lowest lying degenerate conduction band appeared to have a slightly lower minimum near *K*, which actually made the gap *indirect* with a value of 1.69 eV.
[35] The valence band maximum and conduction band minimum occur at $\frac{1}{4}$ and $\frac{3}{4}$, respectively, of the distance between *L* and Γ. It was not possible to give a more accurate location of the indirect gap because of very flat bands in the L-Γ direction.
[36] The DOS was generated by Gaussian smearing with $\sigma = 10$ meV and a $12 \times 12 \times 6$ MP grid using the converged self-consistent charge density obtained with a $2 \times 2 \times 1$ MP grid.
[37] As in the hyperdiamond case, we also find that the lowest lying degenerate conduction band is slightly lower at *K*, giving an indirect gap of 1.52 eV.
[38] V. P. Antropov, O. Gunnarsson, and A. I. Liechtenstein, Phys. Rev. B **48**, 7651 (1993).
[39] M. Côté, J. C. Grossman, M. L. Cohen, and S. G. Louie, Phys. Rev. Lett. **81**, 697 (1998).
[40] I. Spagnolatti, M. Bernasconi, and G. Beneder, Europhys. Lett. **59**, 572 (2002).
[41] C. A. Kuntscher, G. M. Bendele, and P. W. Stephens, Phys. Rev. B **55**, R3366 (1997).
[42] M. M. Ross, H. H. Nelson, J. H. Callahan, and S. W. McElvany, J. Phys. Chem. **96**, 5231 (1992).